



**HAL**  
open science

## Successive reintrusions in a granular medium

B. Darbois Texier, A. Seguin

► **To cite this version:**

B. Darbois Texier, A. Seguin. Successive reintrusions in a granular medium. *Physical Review E* , 2022, 106 (1), pp.014906. 10.1103/PhysRevE.106.014906 . hal-03741175

**HAL Id: hal-03741175**

**<https://hal.science/hal-03741175>**

Submitted on 1 Aug 2022

**HAL** is a multi-disciplinary open access archive for the deposit and dissemination of scientific research documents, whether they are published or not. The documents may come from teaching and research institutions in France or abroad, or from public or private research centers.

L'archive ouverte pluridisciplinaire **HAL**, est destinée au dépôt et à la diffusion de documents scientifiques de niveau recherche, publiés ou non, émanant des établissements d'enseignement et de recherche français ou étrangers, des laboratoires publics ou privés.

# Successive re-intrusions in a granular medium

B. Darbois Texier and A. Seguin

*Université Paris-Saclay, CNRS, Laboratoire FAST, 91405, Orsay, France*

(Dated: August 1, 2022)

We measure and analyze the drag force experienced by a rigid rod that penetrates vertically into a granular medium, partially withdraws before sinking again. The drag during the successive re-intrusions is observed to be significantly smaller than the force experienced in the first run. Two force regimes are evidenced depending on how the re-intrusion depth compares with the withdrawal distance  $\Delta$ . These two regimes are characterized by a force curve of positive and negative curvature and are separated by an inflection point which is characterized experimentally. We approach the difference between the first intrusion and the following re-intrusions by considering a modification in the stress field of the granular material after the partial extraction of the rod. A theoretical model for the stress modification is proposed and allows to rationalize all the experiments realized for different withdrawal distances  $\Delta$ . This framework introduces a crossover length  $\lambda$  above which the stress modification in the granular medium is maintained and that is shown to depend linearly on  $\Delta$ . Finally, the model provides a prediction for the location of the inflection points in reasonable agreement with observations.

## I. INTRODUCTION

Intrusion in a non-cohesive soils is a problem of primary importance for civil engineering, geophysical surveys and animals living in sandy grounds. The development of efficient drilling or probing techniques [1] requires a detailed understanding of the interaction between the intruder and the soil. The survival of animals in sandy environments such as sandfish lizards or sea clams also depends on their capacity to hide beneath the sand surface [2, 3]. In all these situations, the burial of the intruder causes a flow of material [4] and leads to a large vertical resistance that can be seen as a drag force. This drag force has been extensively studied in dry granular media which provide an easy-to-use model soil for modelling these problems.

The drag applied on a rod when it experiences a continuous vertical penetration or extraction in a granular medium at slow speed has already been studied [5]. The force measured during intrusion is an order of magnitude larger than that experienced during extraction. To rationalize these observations, a power law is proposed to describe the quasi-static drag force  $F$  in both directions of motion with the following form  $F/\rho g \pi D^3 = C(z/D)^\lambda$  where  $z$  is the depth of the tip of the intruder,  $D$  its diameter,  $\rho$  the material bulk density,  $g$  the gravity.  $C$  and  $\lambda$  are two non-dimensional coefficients that depend on the direction of motion. For a rod, they measured  $C \simeq 9.5$  and  $\lambda \simeq 1.6$  in penetration,  $C \simeq -0.66$  and  $\lambda \simeq 1.3$  in extraction. In the case of penetration alone, another model has been proposed considering that the drag force comes from the contribution of two terms: one coming from the hydrostatic-like pressure at the tip of the rod  $F \propto z$  and another resulting from the friction applying on the lateral surface  $F \propto z^2$  [6]. Recently, the penetration

of objects at shallow depths has shown the presence of a particular regime where the drag force is closely related to the Archimedean force with a pre-factor that strongly increases with the effective friction coefficient of the granular medium [7, 8]. This hydrostatic-like regime is not dominant as soon as the depth of the intruder becomes large enough, i.e. after a few object diameters ( $z \gtrsim 2D$ ). In the case of extraction, the force corresponds approximately to the weight of the granular column above the object. The asymmetric behaviour of the drag force between intrusion and extrusion phases has also been demonstrated in other experimental studies [9, 10]. This difference is explained by the fact that in extraction the drag force corresponds essentially to friction on the surface of the rod, unlike penetration where most of the force comes from the compression of the packing under the rod, i.e. the increase of the volume fraction under the rod. The geometry of the object has been modified and this difference between penetration and extraction remains similar [11].

Nonetheless, all these studies focus on a single and continuous intrusion or extrusion of the intruder in a granular medium. However, the motion of intruders in practical applications and natural conditions are often more complex than a continuous motion and may include vibrations of small amplitude, rotations and back and forth movements. This is the case in ground drilling where penetration/extraction cycles are required to remove the excess of material and in anchoring problems where the anchor must resist periodic loads [12]. In nature, sea clams use a cyclical movement strategy called "push and pull" to penetrate up to two meters deep into the sediment [3, 13]. On earth, the burrowing worms employ peristaltic waves to progress into non-cohesive substrates [14]. The presence of mechanical vibrations at the surface of the intruder has been proved to fluidize locally the granular medium and to reduce significantly

the intrusion force [15, 16]. Adding a rotational component to the progressive motion has been shown to be an effective strategy for reducing the resistance to intrusion [17] and the drag force of an object moving horizontally [18]. The case of back and forth motions was studied by examining the response of granular materials in a shear cell subjected to repeated cycles [19–23] and to cyclic horizontal motion of an object [24]. These experiments reveal that after shear reversal, the shear stress follows an exponential evolution towards its nominal value which is due to the reorientation of force chains in the medium. However, the effect of back and forth motions on the intrusion force to penetrate a granular medium is under-explored while this configuration cannot be inferred from previous studies because the orientation of gravity changes the flow of material and the structure of the force network. The goal of this study is to fill this gap and consider the force experienced by an intruder in a granular medium as it undergoes a succession of vertical intrusion and extrusion phases.

In this paper, we study experimentally the re-intrusion of a rigid rod after a first intrusion step and a partial extraction. By performing successive cycles of extrusion and re-intrusion of asymmetric amplitude, we evidence two different regimes for the drag force during re-intrusions. Depending on the depth of re-intrusion and the withdrawal distance, the drag can either increase supralinearly or sublinearly with depth. The transition between these two behaviors is characterized by an inflection point in the evolution of the drag force with depth. We first detail the experimental procedure followed to measure the drag force. Then, we present the results that demonstrate the existence of two regimes. Finally, we propose a model based on regularization of the stress in the granular medium after the passage of the intruder and that captures our observations.

## II. EXPERIMENTAL SETUP

The experiments consist in plunging downwards a vertical rigid rod into a dry granular medium (Fig. 1). The rod has a diameter  $D = 12$  mm, a length  $L = 300$  mm and is ended by a conical tip of angle  $60^\circ$ . The rod is made of steel and its surface has been polished to reduce the effect of surface roughness. Granular matter is made of sieved glass beads of diameter  $d = 1$  mm and density  $\rho = 2.5 \times 10^3 \text{ kg.m}^{-3}$ . The dispersion in size for these beads is smaller than 10%. The grains are poured in a cylindrical container of diameter  $D_c = 80$  mm and height 250 mm. In all our experiments, a minimal distance of 50 mm is let between the tip of the rod and the bottom of the container in order to avoid the influence of the bottom wall [25]. The initial prepara-

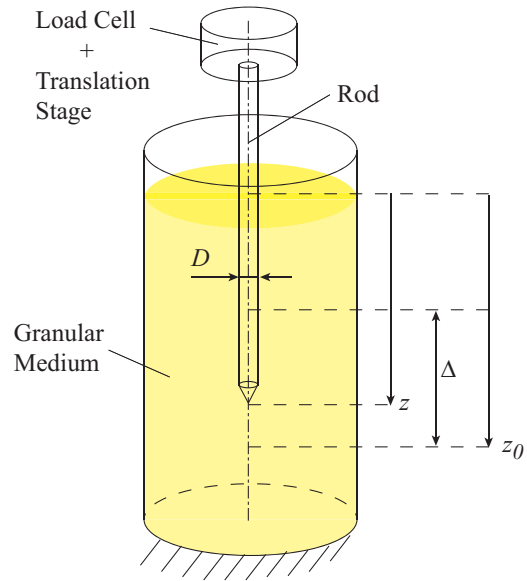


Figure 1. Sketch of the experimental setup and notations.

tion of the granular medium is realized by tapping the containers at least ten times before each experiment, a procedure that permits to reach an initial packing fraction of  $\phi \simeq 0.63$  with a good reproducibility. The rod is mounted on a translation stage that allows a precise control of the vertical displacement of the rod. In our experiments, the intruder velocity  $V_0$  is maintained constant between 0.1 and 1 mm/s which insures to lay in the quasi-static regime where granular forces does not depend on the velocity of the intruder [26, 27]. The vertical force experienced by the rod during its motion is measured with a force sensor placed at the base of the rod and that has a resolution of 10 mN. A typical experiment consists in placing the tip of the intruder just above the horizontal granular surface and plunging the rod up to a given depth  $z_0$  below the surface and then extracting the rod by a withdrawal distance  $\Delta$  before plunging again the rod up to larger depths. Note that the variation of the filling level of the grains corresponds to the volume of immersed rod. This intrusion/extrusion cycles can eventually be repeated several times at different depths  $z_0$  and for different cycle amplitudes  $\Delta$ .

## III. RESULTS

In this study, we consider as a reference case the intrusion of the rod at a constant and low velocity without cycles. A previous study has shown that this force results from two contributions: the hydrostatic-like pressure applying on the tip of the rod and the frictional force exerting along its length [6]. They provided the

following expression for the vertical force  $F_0$  experienced during a continuous intrusion:

$$\frac{F_0}{\pi\phi\rho g D^3/4} = C_1 \left(\frac{z}{D}\right) + C_2 \left(\frac{z}{D}\right)^2 \quad (1)$$

where  $C_1$  and  $C_2$  are non-dimensional coefficients that are determined experimentally. In our system, the vertical force  $F_0$  experienced by the rod as a function of depth  $z$  is shown in figure 2 by the way of a black solid line. The best fit of our data with Eq. (1) is found for  $C_1 = 10 \pm 2$  and  $C_2 = 19 \pm 1$ . These values lay in the same range as previous estimations for flat-ended rods penetrating into glass beads [6].

Due to the finite size effect of the container, possible wall effect generated by friction may be expected [28–30]. However, the effective friction due to the presence of these walls is contained in the value of the coefficients  $C_1$  and  $C_2$  of the equation 1. We therefore expect that the dimensions of the container will influence these two coefficients. We always keep the same container dimensions for all measurements.

#### A. Successive re-intrusions at constant $\Delta$

We are first interested in the resistance experienced by the rod as it undergoes successive intrusion/extrusion cycles for given  $z_0$  and  $\Delta$ . Figure 2 shows the vertical force  $F$  as a function of the intrusion depth  $z$  for the first (black solid line) and nine successive extrusion/intrusion cycles (color solid lines). We observe that when the rod moves upwards, the force decreases over a very short distance, of the order of a millimeter, the diameter of a grain. This behavior is related to the fact that the surface of the rod is smooth and would be different for rough surfaces. Since the extrusion force remains at a very low level during all the extrusion phase, we did not focus on this phase in the following of the study. When the rod moves downwards again (blue solid line), the depth-force curve follows a very different path than the first intrusion and finally recovers the nominal value,  $F_0$ , at the initial depth,  $z \simeq z_0$ . The evolution of the force  $F$  with  $z$  during the successive re-intrusions is clearly below the initial force. In term of energy, the work necessary to re-intrude on a distance  $\Delta$  is about 36 % lower than the initial work required to penetrate on the same distance during the first intrusion. Importantly, we note that all the following cycles do superimpose. This observation is confirmed by the inset of Fig. 2 which presents the relative normalized depth  $(\ell - \ell_0)/D$  as a function of the cycle number  $N$  where  $\ell$  corresponds to the depth for which  $F = 10$  N and  $\ell_0$  to the same quantity when  $N = 0$

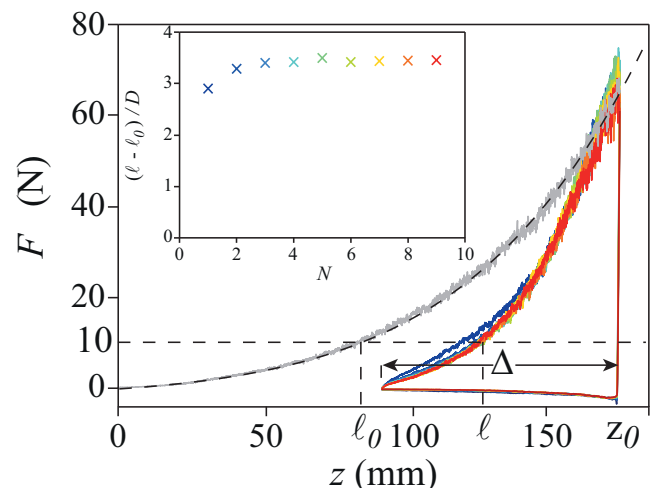


Figure 2. Drag force  $F$  experienced by a rod of diameter  $D = 12$  mm as a function of the depth  $z$  for successive intrusion/extrusion cycles realized for  $z_0 = 170$  mm and  $\Delta = 80$  mm. The rod is displaced at constant velocity  $V_0 = 0.3$  mm.s $^{-1}$  in glass beads of mean diameter  $d = 1$  mm. The gray solid line corresponds to the force experienced during the first continuous intrusion. Color solid lines from blue to red represent the following nine extrusion/intrusion cycles. The dark dashed line corresponds to the best fit of the first intrusion with Eq. (1). The horizontal dash line indicates  $F = 10$  N which intersects the force curves in  $\ell_0$  and  $\ell$  for the first and successive intrusions respectively. Inset:  $(\ell - \ell_0)/D$  as a function of the cycle number  $N$ .

. This graph shows that  $(\ell - \ell_0)/D$  increases with  $N$  before saturating towards a constant value. Finally, the variation of  $(\ell - \ell_0)/D$  after the first re-intrusion remains small (less than 5 % in relative value) and the most significant changes occur during the first intrusion/extrusion cycle. For this reason, we will only consider the first cycle in the following of the article.

#### B. Re-intrusions at different values of $\Delta$

In this section, we focus on the drag force  $F$  as the rod undergoes successive re-intrusion cycles with different amplitudes  $\Delta$  but constant initial intrusion depth  $z_0$ . These results are shown in figure 3 for  $z_0 = 170$  mm and extrusion distances  $\Delta$  ranging from 3 mm to 100 mm. As noted previously, one can notice the significant differences between the first intrusion and the second re-intrusions. For each withdrawal distance  $\Delta$ , the path followed by the re-intrusion force is different and the curves only superimpose when the depth reaches approximately  $z_0$ . At this depth, the re-intrusion force recovers the nominal value experienced during the first intrusion. We remark that the beginning of the re-

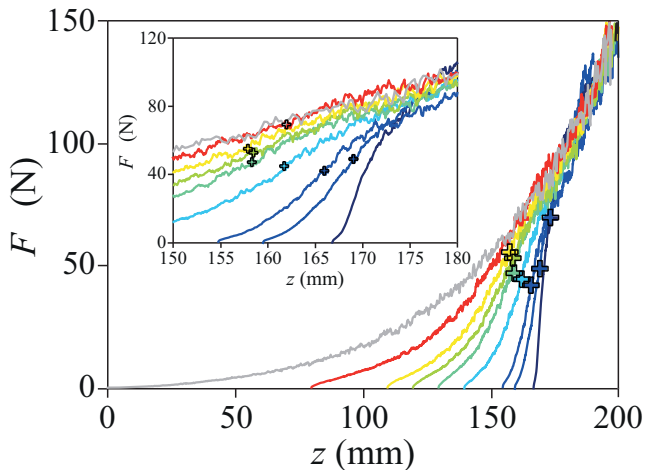


Figure 3. Drag force  $F$  on the rod as a function of the penetration depth  $z$  for different cycle amplitudes  $\Delta$  and a constant initial depth  $z_0 = 170$  mm. Color code spans from blue to red for  $3 \leq \Delta \leq 100$  mm respectively. The black line represents the initial run. Inset: Zoom in of the same data around  $z_0$ . Crosses indicate the inflection points where  $d^2F/dz^2 = 0$ .

intrusion force curve has a similar shape to the curve of the first intrusion with a supralinear growth, corresponding to a positive curvature. At larger re-intrusion depths, the force curve changes in behavior to tangent the initial curve and recovers the same level as during the first intrusion. In this domain, the curvature of the force curve is negative. These two regimes are separated by an inflection point of the force curve, whose depth is noted  $z_i$ . We estimate the location of the inflection point by calculating the curvature of the experimental force curve and determining the depth at which the curvature changes its sign. The results of this procedure are indicated with crosses in Fig. 3. These results are also presented separately in Fig. 4 which shows the normalized depth of the inflection point  $z_i/z_0$  as a function of the normalized withdrawal distance  $\Delta/z_0$ . We observe a decrease of the depth of the inflection point as the withdrawal distance increases before the data become dispersed at large  $\Delta$ . Note that we do not present the extreme case  $\Delta = 170$  mm since the curve obtained is similar to the curve of the first run. To summarize, the re-intrusion curves show two regimes: a first regime where the force growth is similar to the first intrusion and that takes place at the beginning of the re-intrusion ( $z_0 - \Delta < z < z_i$ ) and a second regime where the force inflects toward the initial curve which occurs when  $z$  gets closer to  $z_0$  ( $z_i < z < z_0$ ). Overall, this behavior describes the fact that the effort to partially plunge back into a granular material is weaker at shallow re-intrusion depths but ultimately, the initial force level is recovered as soon as the intruder returns to  $z_0$ .

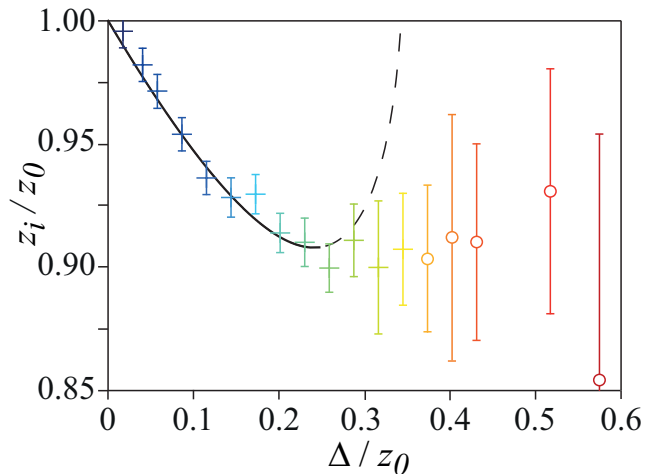


Figure 4. Normalized depth of the inflection point  $z_i/z_0$  as a function of the normalized withdrawal distance  $\Delta/z_0$ . The inflection points (crosses) are deduced from the re-intrusion curves presented in figure 3. The circles represent the measurements where the force curvature at  $z = z_r$  is lower than signal fluctuations and thus the determination of  $z_i$  is uncertain. The prediction of Eq. (5) for  $\lambda = 0.70\Delta$  is represented by solid line for short withdrawal distances and dashed line for large withdrawal distances.

As a consequence, it is illusory to attempt reducing the drag force on a intruder by realizing non-symmetric intrusion/extrusion cycles since the force always recover its nominal value  $F_0$  at the initial depth.

#### IV. DISCUSSION

In order to understand the origin of the force reduction during re-intrusion, we look for a change in the packing fraction of the granular medium along the successive cycles. We deduce the mean packing fraction of the medium by tracking the height of the free surface during intrusion/extrusion cycles. These experiments show that the volume change detected at the free-surface is equal to the volume of the intruder that plunges or retracts from the medium within measurements uncertainties. Thus, the change in the force-curve between first and following intrusions is unlikely to be the result of dilatancy effects but should rather result from stress modification in the medium [31, 32]. The modeling of the drag force on objects in granular media is most often based on the granular resistive force theory [18, 33–37]. In the current experiment, the extraction generates a local decrease of the packing fraction at the end of the stem, creating a flow of grains from dense to less dense zones. Thus, the reorganization of the medium during extraction causes a modification of the initial stress in the granular medium and it is dif-

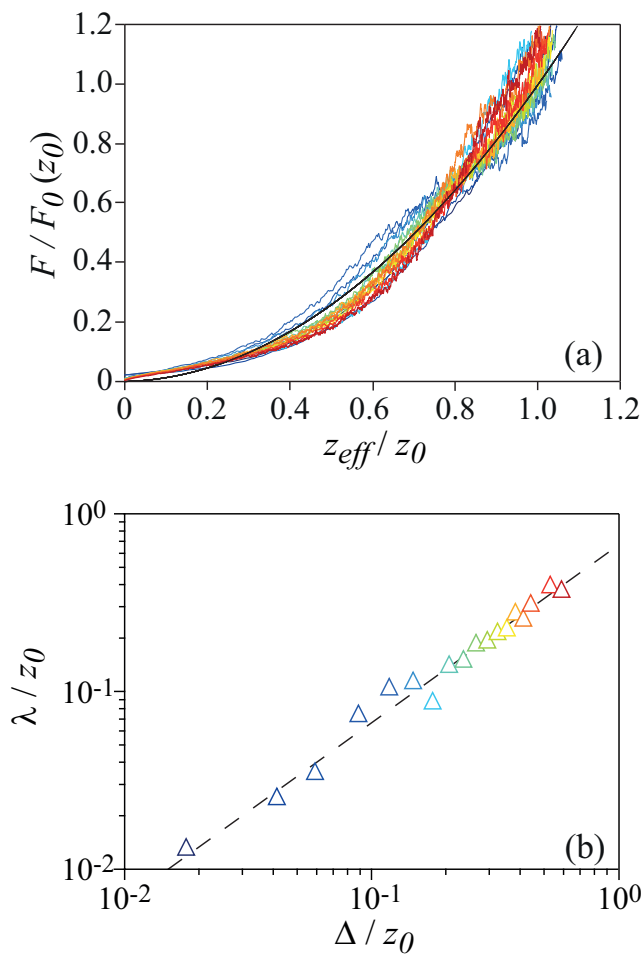


Figure 5. (a) Normalized drag force  $F/F_0(z_0)$  as a function of the normalized effective depth  $z_{\text{eff}}/z_0$ . Color code spans from blue to red for  $3 \leq \Delta \leq 100$  mm respectively. The black line correspond to Eq. (3). (b) Crossover length  $\lambda$  as a function of the re-intrusion depth  $\Delta$ . The dashed line corresponds to the equation  $\lambda/z_0 = 0.70 \Delta/z_0$  and correspond to the best fit of the data.

difficult to place oneself in the framework of this theory.

In the following, we develop a description of the stress  $\sigma_{zz}$  in the granular material along the successive re-intrusions. During the first intrusion up to a depth  $z_0$ , the stress  $\sigma_{zz}$  in the granular column has a hydrostatic-like dependency such that  $\sigma_{zz} \sim \phi \rho g z$ . During the extraction, the intruder returns to a depth  $z_r = z_0 - \Delta$  and granular avalanches fill the wake left by the object during its ascension [38], thus creating a new column of grains. When stopping at a depth  $z_r$ , a free surface is created just below the tip of the intruder, which is compatible with a zero force measured on the intruder at this position (Fig. 2). During re-intrusion, the intruder should experience a new stress that writes  $\sigma_{zz}^{(r)} \sim \phi \rho g (z - z_r)$ , since the free surface is now lo-

cated at  $z_r = z_0 - \Delta$ . However, in the depths of the medium, the stress  $\sigma_{zz}$  still respects  $\sigma_{zz}^{(i)} \sim \phi \rho g z$ . These two states of stress field are not compatible and should be reconciled at intermediate depths. For short extrusion distances  $\Delta$  and large depths  $z_0$ , the depth-force curve is sub-linear and is a concave function (inset of Fig. 3). On the contrary, for large extrusion distances and small depths, the depth-force curve is supra-linear with a positive curvature (Fig. 3). In order to unify the two stress profiles, we suggest a continuous transition between them that is accounted by introducing an effective depth  $z_{\text{eff}}$  which is a weighted average between  $z$  and  $z - z_r$ :

$$z_{\text{eff}} = (z - z_r) e^{-\frac{z - z_r}{\lambda}} + z \left( 1 - e^{-\frac{z - z_r}{\lambda}} \right), \quad (2)$$

where  $\lambda$  is the characteristic length of this transition. Note that the two exponential terms in this relation correspond to an arbitrary choice of weighting functions and do not correspond to a Janssen saturation of the stress in the granular medium. With this definition, the effective depth  $z_{\text{eff}}$  is equals to  $z - z_r$  at small re-intrusion depths ( $z - z_r \ll \lambda$ ) and tends to  $z$  at large depths ( $z - z_r \gg \lambda$ ). Implementing the regularized stress profile  $\phi \rho g z_{\text{eff}}$  in the equation 1, we get the following expression for the re-intrusion drag force:

$$\frac{F(z_{\text{eff}})}{\pi \phi \rho g D^3 / 4} = C_1 \frac{z_{\text{eff}}}{D} + C_2 \left( \frac{z_{\text{eff}}}{D} \right)^2, \quad (3)$$

where  $z_{\text{eff}}$  is given by Eq. (2). This expression can be re-expressed preferably by normalizing the drag force by the initial force at a depth  $z = z_0$ ,  $F_0(z_0)$ , resulting in:

$$\frac{F(z_{\text{eff}})}{F_0(z_0)} = \tilde{C}_1 \frac{z_{\text{eff}}}{z_0} + \tilde{C}_2 \left( \frac{z_{\text{eff}}}{z_0} \right)^2, \quad (4)$$

where  $\tilde{C}_1 = \pi \phi \rho g D^2 C_1 F_0(z_0) z_0 / 4$  and  $\tilde{C}_2 = \pi \phi \rho g D C_2 F_0(z_0) z_0 / 4$ .

This prediction can be compared with our observations realized for different cycle amplitudes (Fig. 3). For this purpose, we consider the crossover length  $\lambda$  as a free parameter and we look for the values that provide the best fit of our data. Figure 5(a) presents the experimental result of the drag force  $F(z_{\text{eff}})$  normalized by the nominal force at a depth  $z_0$ ,  $F_0(z_0)$  as a function of the effective depth  $z_{\text{eff}}$  normalized by the initial depth  $z_0$ . The normalization with respect to the length  $z_0$  is justified by the fact that the re-intrusion force recovers its nominal value around this depth. It can be seen that all the curves of Fig. 3 collapse on a master curve which is the prediction of Eq. (3) with the coefficients  $C_1$  and  $C_2$

determined for the first intrusion (see section III). This collapse proves the validity of the proposed model over the range of parameters investigated in this study. In addition, the characteristic length  $\lambda$  estimated through this procedure is shown as a function of the withdrawal distance  $\Delta$  in Fig. 5(b). We observe a linear relation between  $\lambda$  and  $\Delta$  over two decades which is consistent with the qualitative observations made previously. The best fit of these data with a linear trend provides a slope of  $0.70 \pm 0.05$ .

Besides, this model also gives a prediction for the depth  $z_i$  at which the inflection occurs. The inflection point corresponds mathematically to  $(d^2F/dz^2)_{z=z_i} = 0$  which can be calculated from Eqs. (2) and (3). It leads to an implicit relation for  $z_i$ :

$$2e^{-\frac{z_i - z_r}{\lambda}} + \left( \frac{\lambda - z_i}{z_r} - \frac{C_1 D}{2C_2 z_r} \right) + \left( \frac{\lambda}{z_r} \right)^2 e^{\frac{z_i - z_r}{\lambda}} = 0 \quad (5)$$

with  $z_r = z_0 - \Delta$ . The previous relation has no trivial solution and we solve it numerically. The numerical solution of Eq. (5),  $z_i$ , is plotted in Fig. 4 as a function of  $\Delta$  with a black line where we have assumed that  $\lambda = 0.70 \Delta$  consistently with the fit of our data. We observe that the predicted depth of the inflection point coincides with  $z_0$  for zero withdrawal distances  $\Delta$  and moves closer to the surface when  $\Delta$  increases before falling back  $z_0$  for larger  $\Delta$  (dashed portion of the line in Fig. 4). In addition, no inflection points are expected above a critical withdrawal distance of  $\Delta \simeq 0.34 z_0$ . The predictions of the model are in very good agreement with our measurements for small withdrawal distances ( $\Delta < 0.25 z_0$ ). For larger withdrawal distances, we do not observe experimentally the increase of  $z_i$  with  $\Delta$ , showing the range of application of this model. Concerning the large shrinkage distances  $\Delta > 0.34 z_0$ , we are not able to rule out experimentally the presence of an inflection point because of the existence of experimental noise. However, we distinguish in figure 4, the measurements of  $z_i$  where the initial curvature  $(d^2F/dz^2)_{z=z_r}$  is larger than the mean fluctuations of the force curvature (this situation is indicated by crosses) and where it is smaller (indicated by circles) and the existence of the inflection point is not certain. With this distinction, the disappearance of the inflection point predicted theoretically for  $\Delta/z_0 > 0.34$  is not incompatible with our measurements. Finally, the proposed model is accurate to rationalize our observations at small withdrawal distances  $\Delta/z_0 < 0.25$  and give potential

trends for large  $\Delta$ .

## V. CONCLUSION

In this paper, we focus on the drag force during the re-intrusion of an object into a granular material after its partial extraction. Experiments show that the re-intrusion force at the beginning is significantly lower than the force experienced during the first penetration. When the object regains its initial depth in the medium, this behavior fades and the drag force returns to its nominal level. We evidence two force regimes: a first regime where the re-intrusion force starts from zero and increases rapidly with depth adopting a positive curvature and a second regime where the force bends back to the initial intrusion curve and exhibits a negative curvature. These two regimes are separated by an inflection point which has been characterized experimentally. The transition between these two regimes is rationalized by the introduction of a crossover length  $\lambda$ . This length ensures a continuous transition between the two stress profiles present in the granular packing: the stress profile existing before the initial penetration and the stress profile created during the extraction by the filling of the wake of the object. The predictions of this model compare well to our observations both in term of force curve and location of the inflection point. The crossover length  $\lambda$  is shown to scale linearly with the withdrawal distance  $\Delta$ .

The understanding of the transition between two force regimes during re-intrusion relies on the microscopic properties of the material and the internal structure of the packing. This should motivates future numerical simulations to establish how the stress field in the granular medium evolves during the partial-extrusion and the successive intrusions of an object. Also, it would be interesting to extend the present study in specific regimes where the intruder motion should be faster than the characteristic avalanche time at the tip of the rod and to immersed granular medium where the interstitial fluid flow add further physical ingredients to the problem.

## ACKNOWLEDGMENTS

We are grateful to L. Auffray, J. Amarni, A. Aubertin, C. Manquest and R. Pidoux for the development of the experimental setup. This work is supported by ANR PIA funding: ANR-20-IDEEES-0002.

---

[1] D. Shi, Y. Yang, Y. Deng, and J. Xue, *Granular Matter* **21**, 74 (2019).

[2] R. D. Maladen, Y. Ding, C. Li, and D. I. Goldman, *science* **325**, 314 (2009).

- [3] A. Hosoi and D. I. Goldman, *Annual Review of Fluid Mechanics* **47**, 431 (2015).
- [4] E. Hamm, F. Tapia, and F. Melo, *Physical Review E* **84**, 041304 (2011).
- [5] G. Hill, S. Yeung, and S. A. Koehler, *EPL (Europhysics Letters)* **72**, 137 (2005).
- [6] A. Seguin and P. Gondret, *Physical Review E* **98**, 012906 (2018).
- [7] W. Kang, Y. Feng, C. Liu, and R. Blumenfeld, *Nature Communications* **9**, 1101 (2018).
- [8] Y. Feng, R. Blumenfeld, and C. Liu, *Soft matter* **15**, 3008 (2019).
- [9] M. Schröter, S. Nägle, C. Radin, and H. L. Swinney, *EPL (Europhysics Letters)* **78**, 44004 (2007).
- [10] Z. Peng, X. Xu, K. Lu, and M. Hou, *Phys. Rev. E* **80**, 021301 (2009).
- [11] C. Li, T. Zhang, and D. I. Goldman, *Science* **339**, 1408 (2013).
- [12] T. Hossain and P. Rognon, *Physical Review E* **102**, 022904 (2020).
- [13] A. Winter, R. Deits, D. Dorsch, A. Slocum, and A. Hosoi, *Bioinspiration & Biomimetics* **9**, 036009 (2014).
- [14] K. M. Dorgan, *Journal of Experimental Biology* **218**, 176 (2015).
- [15] B. Darbois Texier, A. Ibarra, and F. Melo, *PLoS ONE* **12**, e0175412 (2017).
- [16] D. Firstbrook, K. Worrall, R. Timoney, F. Suñol, Y. Gao, and P. Harkness, *Proceedings of the Royal Society A: Mathematical, Physical and Engineering Sciences* **473**, 20160673 (2017).
- [17] W. Jung, S. M. Choi, W. Kim, and H.-Y. Kim, *Physics of Fluids* **29**, 041702 (2017).
- [18] A. Seguin, *Physical Review Fluids* **7**, 034302 (2022).
- [19] C. S. Chang, A. Misra, and S. S. Sundaram, *Soil Dynamics and Earthquake Engineering* **10**, 201 (1991).
- [20] J. Sun and S. Sundaresan, *Journal of Fluid Mechanics* **682**, 590 (2011).
- [21] N. Khalili, M. Habte, and S. Valliappan, *International journal for numerical methods in engineering* **63**, 1939 (2005).
- [22] M. Nicolas, P. Duru, and O. Pouliquen, *The European Physical Journal E* **3**, 309 (2000).
- [23] J. Zhang, T. Majmudar, A. Tordesillas, and R. Behringer, *Granular Matter* **12**, 159 (2010).
- [24] A. Seguin, *The European Physical Journal E* **42**, 1 (2019).
- [25] M. B. Stone, R. Barry, D. P. Bernstein, M. D. Pelc, Y. K. Tsui, and P. Schiffer, *Phys. Rev. E* **70**, 041301 (2004).
- [26] R. Albert, M. A. Pfeifer, A.-L. Barabási, and P. Schiffer, *Phys. Rev. Lett.* **82**, 205 (1999).
- [27] L. K. Roth, E. Han, and H. M. Jaeger, *Physical Review Letters* **126**, 218001 (2021).
- [28] G. Ovarlez, E. Kolb, and E. Clément, *Physical Review E* **64**, 060302 (2001).
- [29] Y. Bertho, F. Giorgiutti-Dauphiné, and J.-P. Hulin, *Physical Review Letters* **90**, 144301 (2003).
- [30] L. López-Rodríguez and F. Pacheco-Vázquez, *Physical Review E* **96**, 030901 (2017).
- [31] A. J. Kabla and T. J. Senden, *Physical Review Letters* **102**, 228301 (2009).
- [32] F. Guillard, Y. Forterre, and O. Pouliquen, *Physics of Fluids* **26**, 043301 (2014).
- [33] T. Zhang and D. I. Goldman, *Physics of Fluids* **26**, 101308 (2014).
- [34] B. D. Texier, A. Ibarra, and F. Melo, *Physical Review Letters* **119**, 068003 (2017).
- [35] P. E. Schiebel, H. C. Astley, J. M. Rieser, S. Agarwal, C. Hubicki, A. M. Hubbard, K. Diaz, J. R. Mendelson III, K. Kamrin, and D. I. Goldman, *eLife* **9**, e51412 (2020).
- [36] S. Agarwal, A. Karsai, D. I. Goldman, and K. Kamrin, *Science Advances* **7**, eabe0631 (2021).
- [37] B. D. Texier, A. Ibarra, and F. Melo, *Physical Review Fluids* **6**, 034604 (2021).
- [38] T. Hossain and P. Rognon, *Granular Matter* **22**, 72 (2020).